


# Equivalence between $\omega^n$ Source Time Functions and Those Proposed from Dynamic Finite-Source Modeling

Igor A. Beresnev\*<sup>1</sup> 

## ABSTRACT

There is far-reaching equivalence between the source time functions inferred from dynamic rupture simulations and those corresponding to the kinematic models of slip radiating the generalized omega- $n$  spectrum, in which the power  $n$  is allowed to take on noninteger values. First, the same two physical parameters of faulting—the final-fault displacement  $U$  and the peak rate of slip  $v_m$ —govern the slip law in both cases. Second, in both models, the widths of the radiated far-field velocity pulses follow close analytical forms. Third, the full variety of temporal shapes of the dynamic source time functions, spanning the entire parameter space, closely corresponds to the variation in the omega- $n$  shapes with  $n$  changing from 1.5 to 3.5, approximately. Smaller  $n$  lead to the source time functions that reach the maximum value of slip velocity faster: they cause greater asymmetry of the resulting far-field ground-displacement pulse and shorter duration of the positive velocity pulse. Fourth, in the frequency domain, the  $\omega^n$  spectrum, in which  $n$  changes in a narrower range from approximately 2 to 2.5, similarly includes nearly the entire range of possible dynamic Fourier spectra. The narrower range in  $n$  found in the frequency domain is explained by the constraints on the spectral slope imposed by the specific triangular shape of the dynamic functions. Fifth, in both dynamic and  $\omega^n$  models, the peak rate of slip  $v_m$  is the parameter exerting dominant effect on the strength of fault's high-frequency radiation, in the identical quantitative manner. It follows that the omega- $n$  model of slip, in which  $n$  is allowed to vary, correctly captures the underlying physics of rupture.

## KEY POINTS


- Are slip functions used in kinematic ground-motion models equivalent to those inferred for dynamic ruptures?
- The slip functions corresponding to omega- $n$  models are equivalent to those obtained from dynamic simulations.
- Models of slip that radiates the generalized omega- $n$  spectrum correctly capture the underlying rupture physics.

## INTRODUCTION

Prescribing the temporal shape of slip on causative faults (the source time function) is one of the crucial components in the models of synthesizing future ground motions for seismic hazards. Such function is nonetheless one of the most poorly observationally constrained characteristics of faulting. The early classic kinematic models of earthquake radiation introduced the source time (slip) function that is as simple as a linear ramp, known as the Haskell model (Aki and Richards, 1980, their equation 14.19). In this case, the temporal dependence of slip velocity (the time derivative of source displacement) is a rectangle. Because the slip velocity (not fault

displacement itself) controls the far-field radiation, the literature has focused on choosing the other alternative acceptable shapes of the slip-velocity functions (SVFs).

The models of source slip in kinematic ground-motion simulations have often assumed the temporal functions that radiate the Fourier spectrum of seismic displacement into the far field having the “ $\omega^n$ ” shape. Such an amplitude spectrum is flat at low frequencies and falls off as  $-n$  beyond its corner frequency. The classic examples include the exponential rise to static displacement ( $n = 1$ ) (Aki and Richards, 1980, p. 810) or the Brune SVF ( $n = 2$ ) (Brune, 1970, his equation 17). Beresnev (2019, his equation 4) found that all omega- $n$  source time functions, for any real (not necessarily integer) positive  $n$  could be encompassed by a single formula,

1. Department of Geological & Atmospheric Sciences, Iowa State University, Ames, Iowa, U.S.A.,  <https://orcid.org/0000-0002-4050-919X> (IAB)

\*Corresponding author: beresnev@iastate.edu

**Cite this article as** Beresnev, I. A. (2022). Equivalence between  $\omega^n$  Source Time Functions and Those Proposed from Dynamic Finite-Source Modeling, *Bull. Seismol. Soc. Am.* **112**, 1886–1893, doi: [10.1785/0120210284](https://doi.org/10.1785/0120210284)

© Seismological Society of America

$$\Delta u_n(t) = U \left[ 1 - \frac{\Gamma(n, t/\tau)}{\Gamma(n, 0)} \right], \quad t \geq 0, \quad (1)$$

in which  $\Delta u_n(t)$  is the fault slip,  $U$  is its final (static) value, and  $\Gamma(a, x)$  is the incomplete gamma function [ $\Gamma(a, x) = \int_x^\infty e^{-t} t^{a-1} dt$ ]. The quantity  $\tau$  is the time scale, related to the physical parameters of faulting  $U$  and  $v_m$  as

$$\tau = \frac{(n-1)^{n-1} U}{(n-1)! e^{n-1} v_m}, \quad (2)$$

in which  $v_m$  is the maximum velocity of slip (Beresnev, 2001, his equation 3; Beresnev, 2019, his equation 8). Here, the factorial is resolved through the gamma function  $\Gamma(n) = (n-1)!$ . The quantity  $\tau$  controls the value of the corner frequency of the radiated omega- $n$  spectrum  $\omega_c = 1/\tau$ . Smaller  $n$  in the functional series in equation (1) lead to the source time functions that reach the maximum value of slip velocity  $v_m$  faster: they cause greater asymmetry of the resulting far-field ground-displacement pulse and shorter duration of the positive velocity pulse.

The conceptual equation (1) captures the essence of fault slip, in that it begins at zero, rises to achieve the maximum velocity, and then gradually approaches the static value (e. g., fig. 1 of Beresnev, 2019). It allows for the fact that fault movement never in reality stops, continuing to indefinitely creep at a very small rate.

The slip velocity (the derivative of equation 1) is

$$\Delta \dot{u}_n(t) = \frac{U}{(n-1)! \tau} \left( \frac{t}{\tau} \right)^{n-1} e^{-t/\tau} \quad (3)$$

(Beresnev and Atkinson, 1997, their equation 8; Beresnev, 2019, his equation 5). Functions from the equations (1) or (3) have been commonly utilized in ground-motion prediction, especially the  $\omega^2$  shape in the popular stochastic method (Beresnev and Atkinson, 1997; Boore, 2003; Motazedian and Atkinson, 2005; Mena *et al.*, 2010); however, they do not follow from rigorous physical solutions.

Fault-displacement functions have also been proposed that follow from dynamic simulations of earthquake ruptures. Such solutions cannot be considered a satisfactory alternative either. Dynamic simulations have to specify numerous laws and physical parameters that are largely unconstrained by observations and have to be virtually guessed. Examples include the details of dynamic and static fault friction, fracture energies, stresses acting on fault planes, material rheology and stress concentrations at the fracture tip, as well as spatial heterogeneity in all these quantities. A well-known deficiency of the rigorous linear-elastic fracture mechanics is its inability to remove stress singularities from the tips of the cracks. The often phenomenological approximations that have to be made, albeit helping clarify the physics, have not reached the stage of being able to reliably supplant in their accuracy the kinematic

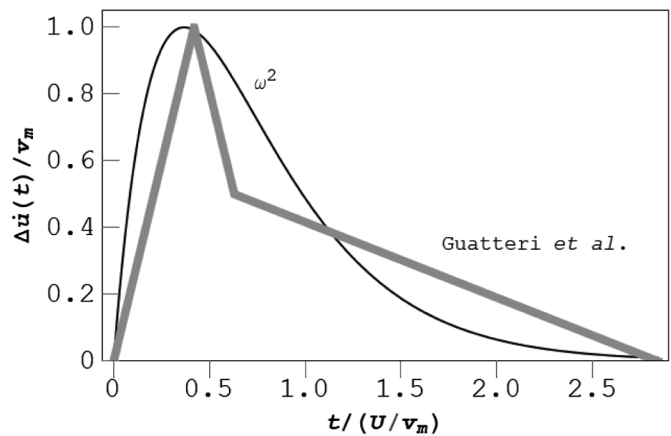


**Figure 1.** Comparison of the “standard” pseudodynamic ( $\beta_1 = 0.84$  and  $c = \frac{1}{2}$ ) and the  $\omega^2$  slip-velocity functions (SVFs).

models that make reasonable assumptions about the slip functions (e.g., Graves and Pitarka, 2010, p. 2095). The kinematic models have been adopted as the Broadband Platform (BBP) for ground-motion simulation by the Southern California Earthquake Center (SCEC) (Dreger and Jordan, 2015). They do benefit from established features of dynamic solutions (Graves and Pitarka, 2010; Pitarka *et al.*, 2022).

Guatteri *et al.* (2004) made an effort to summarize and parameterize the functional forms of slip-rate functions that were produced by a large number of dynamic simulations. Because their model is an approximate generalization, they called it “pseudodynamic.” Other studies have also proposed similar dynamically compatible generalizations (e.g., Tinti *et al.*, 2005; Liu *et al.*, 2006). All three formulations are approximately equivalent (Graves and Pitarka, 2010, their fig. 3). It is our goal here to probe the compatibility of the SVFs as represented by the Guatteri *et al.* model with the  $\omega^n$  functional shape (equations 1 and 3) commonly used in kinematic simulations.

## THE PSEUDODYNAMIC AND $\omega^n$ SOURCE TIME FUNCTIONS

### Form of the functions

**Pseudodynamic form.** The shape of the generalized slip-rate function deduced by Guatteri *et al.* is represented in their figure 4: it is composed of two overlapping triangles, an isosceles one (the main pulse) and a rectangular one (the tail) (see e.g., in Figs. 1, 2 subsequently). The heights of the main and the tailing triangles are  $v_m$  and  $c v_m$ , respectively, in which  $c$  is allowed to vary ( $0 < c < 1$ ). The free parameters used are encapsulated in the authors’ equations (8), (11), and (13): they are  $v_m$ ,  $U$ ,  $c$ , and  $\beta_1$ . The quantity  $\beta_1$  is defined in the authors’ equation (11):

$$T_p = \beta_1 \frac{U}{v_m}, \quad (4)$$

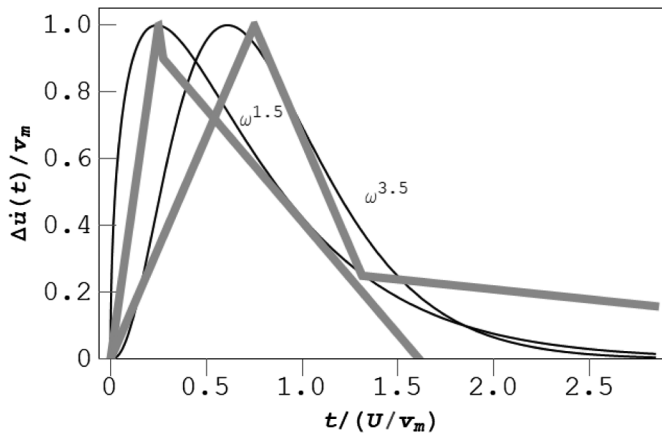


**Figure 2.** The approximate range of change in the shapes of the pseudodynamic and  $\omega^n$  SVFs. The end-member cases are shown: from  $\beta_1 = 0.5, c = 9/10$  ("short pulse, high tail") to  $\beta_1 = 1.5, c = 1/4$  ("wide pulse, low tail") for the pseudodynamic function, and from  $n = 1.5$  to  $n = 3.5$  for the  $\omega^n$  function.

in which they term  $T_p$  the "pulse width" (p. 2055) and equate it to the base of the main triangle (their fig. 4). One can see that  $\beta_1$  is equivalent to the coefficient  $(n-1)^{n-1}/[(n-1)!e^{n-1}]$  in equation (2), and that the time constant  $\tau$  in equation (2) characterizes the pulse width.

We have recast the shape of the triangles through these four parameters. The complete form of the pseudodynamic SVF becomes:

$$\Delta\dot{u}(t) = \frac{2}{\beta_1} v_m \frac{t}{(U/v_m)}, \quad 0 \leq t < \frac{\beta_1 U}{2 v_m}, \quad (5a)$$

$$\Delta\dot{u}(t) = 2v_m \left[ 1 - \frac{1}{\beta_1} \frac{t}{(U/v_m)} \right], \quad \frac{\beta_1 U}{2 v_m} \leq t < \beta_1 \left( 1 - \frac{c}{2} \right) \frac{U}{v_m}, \quad (5b)$$

$$\Delta\dot{u}(t) = \frac{\beta_1 + \frac{1}{c}}{\frac{\beta_1}{2} + \frac{1}{c}} v_m \left[ 1 - \frac{1}{(\beta_1 + \frac{1}{c})} \frac{t}{(U/v_m)} \right], \quad \beta_1 \left( 1 - \frac{c}{2} \right) \frac{U}{v_m} \leq t \leq \left( \beta_1 + \frac{1}{c} \right) \frac{U}{v_m}. \quad (5c)$$

The upper time limit in equation (5c) corresponds to the total SVF duration of  $(\beta_1 + 1/c)U/v_m$  defined by Guatteri *et al.* (see equation 11). For an arbitrary duration  $\tau_r$ , equation (5c) should be replaced by

$$\Delta\dot{u}(t) = \frac{cv_m}{\tau_r - \beta_1(1 - \frac{c}{2})\frac{U}{v_m}} (\tau_r - t), \quad \beta_1 \left( 1 - \frac{c}{2} \right) \frac{U}{v_m} \leq t \leq \tau_r. \quad (5d)$$

It is also convenient to reduce equation (5a)–(5d) to a non-dimensional form through the dimensionless time  $t_1 = t/(U/v_m)$ :

$$\frac{\Delta\dot{u}(t_1)}{v_m} = \frac{2}{\beta_1} t_1, \quad 0 \leq t_1 < \frac{\beta_1}{2}, \quad (6a)$$

$$\frac{\Delta\dot{u}(t_1)}{v_m} = 2 \left( 1 - \frac{1}{\beta_1} t_1 \right), \quad \frac{\beta_1}{2} \leq t_1 < \beta_1 \left( 1 - \frac{c}{2} \right), \quad (6b)$$

$$\frac{\Delta\dot{u}(t_1)}{v_m} = \frac{\beta_1 + \frac{1}{c}}{\frac{\beta_1}{2} + \frac{1}{c}} \left[ 1 - \frac{1}{(\beta_1 + \frac{1}{c})} t_1 \right], \quad \beta_1 \left( 1 - \frac{c}{2} \right) \leq t_1 \leq \left( \beta_1 + \frac{1}{c} \right), \quad (6c)$$

$$\frac{\Delta\dot{u}(t_1)}{v_m} = \frac{c}{\frac{\tau_r}{(U/v_m)} - \beta_1(1 - \frac{c}{2})} \left[ \frac{\tau_r}{(U/v_m)} - t_1 \right], \quad \beta_1 \left( 1 - \frac{c}{2} \right) \leq t_1 \leq \frac{\tau_r}{(U/v_m)}. \quad (6d)$$

It is important to recognize that the Guatteri *et al.* functional shape (equation 5) is parameterized through the same physical quantities  $U$  and  $v_m$  as the omega- $n$  slip function (equations 1 and 2). On the other hand, the Tinti *et al.* pulse was produced from the original Yoffe source time function by formally convolving the latter with a triangle to remove the singularity at the rupture front. This procedure involved an artificially introduced smoothing time window equal to the half-duration of the triangle. The length of the window becomes an inherent but not strictly physical regularization parameter that ultimately controls the resulting ground-velocity pulse. This is a conceptual disadvantage of the Tinti *et al.* formulation that is absent from Guatteri *et al.*'s, whose free parameters carry intuitively clear physical or geometrical meaning. Another methodological disadvantage is that the velocity pulse in this formulation is not analytically integrable to obtain the corresponding time history of slip (Graves and Pitarka, 2010, p. 2098).

The Liu *et al.* functional form (their equations 7a and 7b, reproduced in more detailed form by Aagaard *et al.*, 2010, their equations 5–10) was derived from Guatteri *et al.*'s result but approximated by trigonometric functions. The important distinction with the original Guatteri *et al.* model is that  $v_m$ , the physical parameter of faulting that cannot take on arbitrarily large values (e.g., Beresnev, 2022), was replaced by the subfault rise time in Liu *et al.*'s modification. In our view, such a new formulation may implicitly lead to unrealistically large slip rates, a potential pitfall that their model no longer controls. The fact that the chosen pulse width in their approach strongly affects the shape of the resulting radiation spectra has also been noted by Mena *et al.* (2010, pp. 2146–2147).

The rise time on faults is controlled, on average, by the earthquake magnitude (e.g., Kanamori and Anderson, 1975, the dynamic-similarity condition in their equation 10) and

hence cannot be taken as a truly independent parameter. An additional disadvantage of the Liu *et al.* formulation is that it puts the time at which the maximum slip velocity occurs at a fixed fraction of the total duration  $\tau_r$ , thus losing the inherent flexibility in the SVF shapes allowed in the original Guatteri *et al.*'s form.

For the multiple reasons mentioned, we chose the Guatteri *et al.* original model as the basis for our comparisons. Their SVF has been tested and used without modifications in the deterministic broadband simulations of strong ground motions (e.g., Skarlatoudis *et al.*, 2015, their fig. 1).

The equations for slip velocity (equation 6) are time integrated to fault displacement to obtain:

$$\frac{\Delta u(t_1)}{U} = \frac{1}{\beta_1} t_1^2, \quad 0 \leq t_1 < \frac{\beta_1}{2}, \quad (7a)$$

$$\frac{\Delta u(t_1)}{U} = 2t_1 \left(1 - \frac{1}{2\beta_1} t_1\right) - \frac{1}{2}\beta_1, \quad \frac{1}{2} \leq t_1 < \beta_1 \left(1 - \frac{c}{2}\right), \quad (7b)$$

$$\frac{\Delta u(t_1)}{U} = ct_1 \frac{2(\beta_1 + \frac{1}{c}) - t_1}{2(\beta_1 \frac{c}{2} + \frac{1}{c})} + \frac{\beta_1 [2(1 - 2c) - c^2(\beta_1 - 1)]}{2(2 + c^2\beta_1)},$$

$$\beta_1 \left(1 - \frac{c}{2}\right) \leq t_1 \leq \left(\beta_1 + \frac{1}{c}\right), \quad (7c)$$

$$\frac{\Delta u(t_1)}{U} = ct_1 \frac{1 - \frac{t_1}{2\tau_r/(U/v_m)}}{1 - \frac{\beta_1(1-\frac{c}{2})}{\tau_r/(U/v_m)}} + \frac{\beta_1}{2} \left[1 - \frac{c^2}{2} - c \left(1 - \frac{c}{2}\right) \frac{2 - \frac{\beta_1(1-\frac{c}{2})}{\tau_r/(U/v_m)}}{1 - \frac{\beta_1(1-\frac{c}{2})}{\tau_r/(U/v_m)}}\right],$$

$$\beta_1 \left(1 - \frac{c}{2}\right) \leq t_1 \leq \frac{\tau_r}{(U/v_m)}. \quad (7d)$$

$\omega^n$  form. For comparison with equations (5) and (6), we recast the velocity pulse (equation 3) of the general omega- $n$  model in the explicit form through the same faulting parameters  $v_m$  and  $U$ :

$$\Delta \dot{u}_n(t) = \frac{[(n-1)!]^{n-1} e^{n(n-1)}}{(n-1)^{n(n-1)}} v_m \left[ \frac{t}{(U/v_m)} \right]^{n-1} \times \exp \left[ -\frac{(n-1)! e^{n-1}}{(n-1)^{n-1}} \frac{t}{(U/v_m)} \right], \quad (8)$$

and in the nondimensional form,

$$\frac{\Delta \dot{u}_n(t_1)}{v_m} = \frac{[(n-1)!]^{n-1} e^{n(n-1)}}{(n-1)^{n(n-1)}} t_1^{n-1} \exp \left[ -\frac{(n-1)! e^{n-1}}{(n-1)^{n-1}} t_1 \right]. \quad (9)$$

**Rise time.** The total duration of the pseudodynamic slip-rate pulse, including both triangles, is termed the “rise time” by Guatteri *et al.* denoted by  $\tau_r$ . They arrive at the following equation for the rise time (their equation 13):

$$\tau_r = T_p + \frac{U}{cv_m}, \quad (10)$$

which using equation (4), is transformed into

$$\tau_r = \left(\beta_1 + \frac{1}{c}\right) \frac{U}{v_m}. \quad (11)$$

Guatteri *et al.*'s preferred values of  $\beta_1$  and  $c$  are  $\beta_1 = 0.84$  (their equation 11) and  $c = \frac{1}{2}$  (p. 2056); in the following, we will hence call them the “standard” values. Using them in equation (11) yields

$$\tau_r = 2.84 \frac{U}{v_m}. \quad (12)$$

On the other hand, the rise time of the omega- $n$  slip function (equation 1) can be defined as the period over which the dislocation grows to  $0.99 U$ . The rise time  $\tau_r$  in this case is found as the root of the equation  $1 - \Gamma(n, t/\tau)/\Gamma(n, 0) = 0.99$ . For example, solving it for  $n = 2$  (the commonly used omega-square model), we find  $\tau_r/\tau = 6.64$ . Thus the rise time for the omega-square model, equivalent to equation (12), is

$$\tau_r = 6.64\tau = 2.44 \frac{U}{v_m}, \quad (13)$$

in which the value of  $\tau$  for  $n = 2$  was substituted from equation (2). Comparing equation (13) with (12) shows that the rise time for the omega-square slip is closely equivalent to the pseudodynamic case of Guatteri *et al.*

**Comparison between the functions.** Figure 1 compares the pseudodynamic SVF for the standard values of  $\beta_1 = 0.84$  and  $c = \frac{1}{2}$  (equation 6) with the  $\omega^n$  one for  $n = 2$  (equation 9). We chose  $n = 2$  as the reasonable equivalent to the “standard” pseudodynamic condition, as this value of  $n$  likewise corresponds to a widely accepted omega-square model. The two curves clearly are similar, and both exhibit the presence of the main pulse and the tail.

The shapes of the triangles in the pseudodynamic model vary within the range of the possible values of  $\beta_1$  and  $c$ . Based on figure 5 of Guatteri *et al.*, the representative range of change in the pulse-width coefficient  $\beta_1$ , obtained from a variety of dynamic simulations, excluding extremes, is between approximately 0.5 (“short” pulse) and 1.5 (“wide” pulse). The end-member cases of the triangle shapes, characterizing the possible variety, can thus be reasonably set as  $\beta_1 = 0.5$  and

$c = 9/10$  (“short pulse, high tail”), on one hand, and  $\beta_1 = 1.5$  and  $c = 1/4$  (“wide pulse, low tail”), on the other. These two functions are plotted in Figure 2 in gray color. Dynamic simulations conducted by Pitarka *et al.* (2022, their fig. 6) have reproduced a similar range of patterns of the slip-rate functions.

The full variety in the shapes of the  $\omega^n$  SVF can be characterized by the values of  $n$  from 1.5 to 3.5, approximately. These are plotted in Figure 2 as well as black lines. The comparison with the pseudodynamic SVFs shows close similarity between the respective end-member pairs.

The static value of  $\Delta u(t_1)/U$  in equation (7c) at  $t_1 = \beta_1 + 1/c$  should be equal to one. However, substitution shows that this value is  $(1 + \beta_1)/2$ ; in other words, the Guatteri *et al.* SVFs do not preserve the prescribed final slip. Namely, at the representative values of  $\beta_1 = 0.5, 0.84,$  and  $1.5$  that we have used, the final-fault slip is  $0.75U, 0.92U,$  and  $1.25U,$  respectively. On the other hand, the  $\omega^n$  source time functions do not display such as undesirable behavior. To illustrate, Figure 3 compares the slip functions corresponding to the SVFs from Figure 1. The  $\omega^2$  slip is taken from equation (1) for  $n = 2$ , in which case equation (1) reduces to  $\Delta u(t) = U[1 - (1 + t/\tau) \exp(-t/\tau)]$  (Beresnev and Atkinson, 1997, their equation 6) and is plotted here in the nondimensional form. The standard dynamic slip is represented by equations (7). It is seen that the dynamic solution underpredicts the static slip, which in this case equals  $0.92U$ . The inability of the Guatteri *et al.* pseudodynamic solutions to correctly match the prescribed levels of final-fault displacement is their conspicuous drawback, absent from the  $\omega^n$  solutions.

### Spectra of the functions

**Fourier spectrum of the pseudodynamic function.** It is also important to test the equivalence of the pseudo-dynamic and  $\omega^n$  source time functions in the frequency domain. The complex Fourier transform of the nondimensional SVF (equation 6), calculated as

$$\int_0^{(\beta_1+1/c)} \frac{\Delta \dot{u}(t_1)}{v_m} \exp(-i\omega_1 t_1) dt_1, \quad (14)$$

is

$$\Delta \dot{u}(\omega_1) = \frac{2e^{-i\beta_1 \omega_1} [-2e^{i c \beta_1 \omega_1/2} - c^2 \beta_1 e^{-i\omega_1/c} + (2 + c^2 \beta_1) e^{i\beta_1 \omega_1/2} (2 - e^{i\beta_1 \omega_1/2})]}{\beta_1 (2 + c^2 \beta_1) \omega_1^2}, \quad (15)$$

in which  $\omega_1$  is the dimensionless frequency, and that of the dimensional SVF (equation 5), calculated as  $\int_0^{(U/v_m)(\beta_1+1/c)} \Delta \dot{u}(t) \exp(-i\omega t) dt$ , is

$$\Delta \dot{u}(\omega) = - \frac{2 \exp \left[ -\frac{iU(1+c\beta_1)\omega}{cv_m} \right] v_m^2 \left\{ 2 \exp \left[ \frac{iU(2+c^2\beta_1)\omega}{2cv_m} \right] + c^2 \beta_1 + (2 + c^2 \beta_1) \left\{ \exp \left[ \frac{iU(1+c\beta_1)\omega}{cv_m} \right] - 2 \exp \left[ \frac{iU(2+c\beta_1)\omega}{2cv_m} \right] \right\} \right\}}{U \beta_1 (2 + c^2 \beta_1) \omega^2}. \quad (16)$$

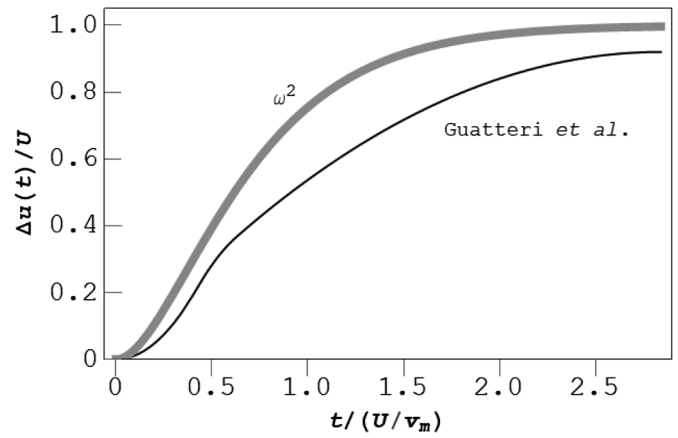


Figure 3. The slip functions corresponding to SVFs in Figure 1.

**Fourier spectrum of the  $\omega^n$  function.** The spectrum of the nondimensional SVF (equation 9) is

$$\Delta \dot{u}_n(\omega_1) = \frac{[(n-1)!]^n e^{n(n-1)} \left[ i\omega_1 + \frac{(n-1)! e^{n-1}}{(n-1)^{n-1}} \right]^{-n}}{(n-1)^{n(n-1)}}, \quad (17)$$

and the spectrum of the dimensional velocity pulse in equations (3) and (8) takes the familiar compact omega- $n$  form:

$$\Delta \dot{u}_n(\omega) = U(1 + i\omega\tau)^{-n}, \quad (18)$$

$$|\Delta \dot{u}_n(\omega)| = U \left[ 1 + \left( \frac{\omega}{\omega_c} \right)^2 \right]^{-n/2}. \quad (19)$$

**Comparison between the spectra.** The nondimensional Fourier amplitude spectra of SVFs presented in Figures 1 and 2 are compared in Figure 4. The pseudodynamic spectra are shown in color, whereas the  $\omega^n$  ones in shades of gray, with  $n$  changing here from 1.5 to 2.5, the middle curve being the case of  $n = 2$ . The units on the frequency axis in Figure 4

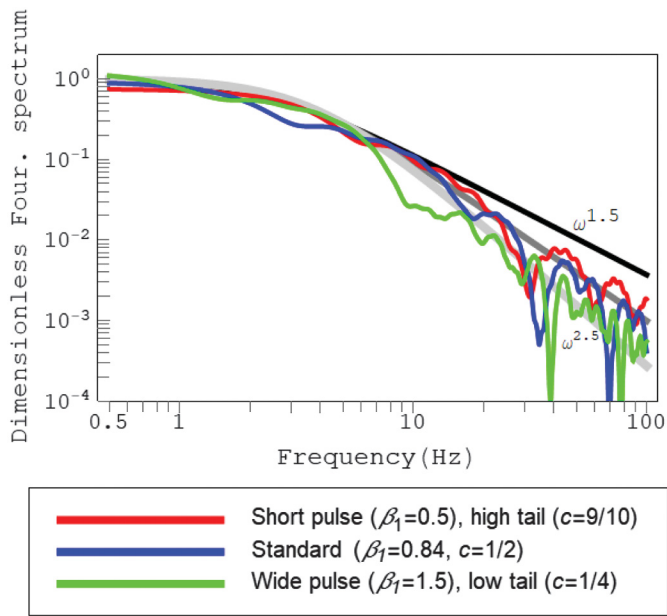


**Figure 4.** Comparison of Fourier amplitude spectra of pseudodynamic and  $\omega^n$  SVFs presented in Figures 1 and 2. The pseudodynamic curves are shown in color and the  $\omega^n$  ones in shades of gray.

are for convenience given in hertz, even though the spectra in equations (15) and (17) are expressed through the dimensionless frequency  $\omega_1$ . Rewriting the exponent in the Fourier transform equation (14) as  $\exp(-i\omega_1 t_1) = \exp[-i\omega_1 t / (U/v_m)] = \exp(-i\omega t)$ , we find the requisite relationship between  $\omega$  and  $\omega_1$ :  $\omega = \omega_1 / (U/v_m)$ . The parameters  $U$  and  $v_m$  are needed to convert the dimensionless frequency to the dimensional  $\omega$ . Accordingly, the example of Figure 4 was produced for an  $M_w$  5 earthquake, with the fault offset  $U = 0.14$  m calculated as  $U = M_0 / (\mu A)$ , in which the seismic moment  $M_0$  was obtained from the moment magnitude  $M_w$  and the fault area  $A$  from the empirical relationship between the rupture area and the moment magnitude (Wells and Coppersmith, 1994, their table 2A). The shear modulus  $\mu$  was calculated as  $\mu = \beta^2 \rho$ , in which the density  $\rho$  was taken as 2700 kg/m<sup>3</sup> and the shear-wave velocity  $\beta$  obtained from the  $P$ -wave velocity of 5000 m/s as  $\beta = 5000 / \sqrt{3}$  m/s. A typical value of  $v_m = 1$  m/s was adopted (Beresnev, 2022). To better observe the high-frequency slopes, the frequency range has been extended to 100 Hz.

One can observe that the  $\omega^n$  spectral model, in which  $n$  changes from approximately 2 to 2.5 (within the space around the two lighter-gray lines in Fig. 4) encompasses nearly the entire range of the possible pseudodynamic spectra.

The range of change in  $n$  (2–2.5), compatible with the full range of pseudodynamic spectra, is narrower than that (1.5–3.5) derived from comparing the temporal shapes in Figure 2. In understanding the origin of this difference, one should recall that Guatteri *et al.*'s dynamic SVFs carry an imposed triangular shape. The amplitude spectrum of an isosceles triangle has the

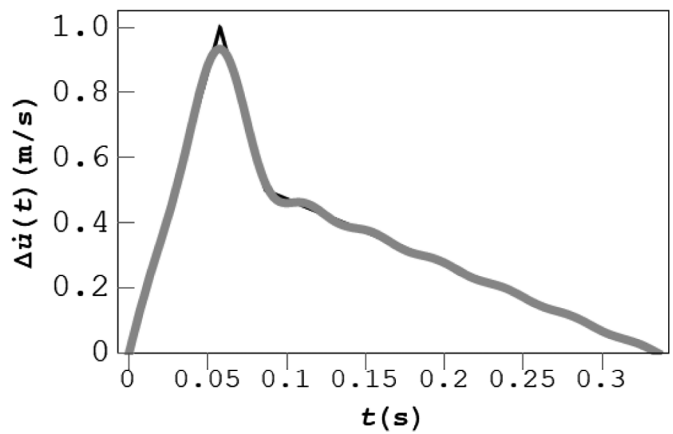


**Figure 5.** Comparison of the “standard” pseudodynamic SVF ( $\beta_1 = 0.84$  and  $c = \frac{1}{2}$ ) with its smooth version obtained from its Fourier expansion retaining 15 first harmonic terms.

$\omega^{-2}$  high-frequency spectral decay: the specific high-frequency content is prescribed by the need to preserve the sharp corners of the triangles. One can expect, for example, that smoothing the triangles will modify the high-frequency slope.

To examine the effect of smoothing on the resulting frequency spectra, it is convenient to decompose the SVF, defined in equations (5a), (5b), and (5d) on the general interval 0 to  $\tau_r$ , into its Fourier expansion by sine functions:

$$\Delta \dot{u}(t) = \sum_{k=0}^{\infty} b_k \sin \frac{k\pi t}{\tau_r}, \quad (20)$$

in which

$$b_k = \frac{2}{\tau_r} \int_0^{\tau_r} \Delta \dot{u}(t) \sin \frac{k\pi t}{\tau_r} dt \quad (21)$$

(Bronshtein *et al.*, 2004, their equation 7.112c). Integration in equation (21) yields the Fourier coefficients

$$b_k = \frac{8v_m}{p\pi^2 k^2} \left[ \sin\left(\frac{p}{2}k\pi\right) + \frac{1-p}{(c-2)p+2} \sin\left(\frac{c-2}{2}pk\pi\right) \right], \quad (22)$$

in which the parameter  $p$  is defined as  $p \equiv (\beta_1/\tau_r)(U/v_m)$ . Considering equation (4),  $p$  has the meaning of the fraction of the pulse width  $T_p$  relative to the rise time  $\tau_r$ .

An infinite number of harmonics in the series (equation 20) are formally needed to exactly reproduce the shape of the triangles. As described by the Gibbs phenomenon (Báth, 1974, his section 2.1.2), the fewer harmonics are retained, the smoother the shape. Figure 5 compares the shape of the exact standard pseudodynamic SVF with its approximate form obtained from expansion (20) when only 15 harmonics have been used in the sum ( $k$  increasing from zero to 15). The

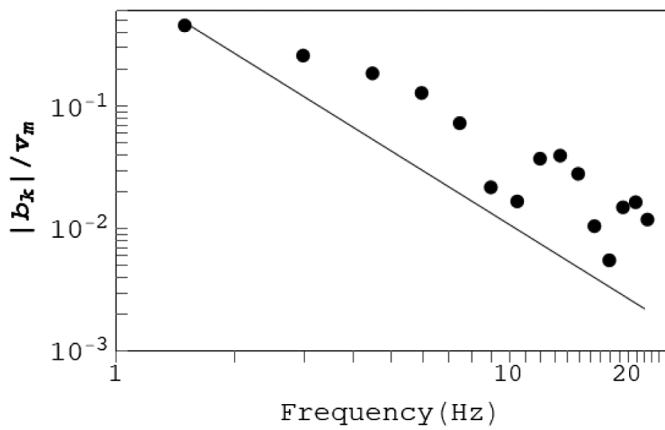


**Figure 6.** The moduli of the amplitudes of the first 15 harmonics in equation (22).

graphs have been plotted to  $\tau_r$  on the horizontal axis, determined from equation (13) using the same values of  $U$  and  $v_m$  as for producing Figure 3 ( $\tau_r = 2.44 \times 0.14/1 = 0.34$  s). The highest frequency in the expansion (equation 20) at  $k = 15$  is 22 Hz. Figure 5 demonstrates that 15 harmonics are sufficient to nearly completely recover the original triangular shape by its smoother variant, except the presence of the sharp corners that do not represent physically realistic features.

The moduli of the amplitudes  $b_k$  of the 15 harmonics represented in Figure 5, calculated from equation (22) and normalized by  $v_m$ , to render them in a dimensionless way, are shown by the filled circles in Figure 6. The solid line indicates the slope of  $-2$ , expected for the exact triangular shape. The pattern defined by the circles follows the slope that is conspicuously less than  $-2$ , indicating that smoothing the triangles modifies the frequency fall-off in the spectral domain, the specific decay being a function of the degree of smoothing. With no smoothing applied, the slope can be expected to be close to  $-2$ , as observed for the exact triangular shapes in Figure 4 explaining the relative clustering of their Fourier spectra.

**Comparison of high-frequency radiation.** In the omega- $n$  model, the parameter that controls the strength of fault's high-frequency radiation is the maximum slip rate  $v_m$  (e.g., Beresnev, 2022). The  $\omega \gg \omega_c$  asymptotics of equation (19) is

$$|\Delta \dot{u}_n(\omega)| = \frac{[(n-1)!]^n e^{n(n-1)} v_m^n}{(n-1)^{n(n-1)} U^{n-1}} \omega^{-n}, \quad (23)$$

in which the expression for  $\omega_c$  from equation (2) has been utilized. It follows that, for given earthquake magnitude (the value of  $U$ ), there is a strong power-of- $n$  dependence of the high-frequency spectral level on  $v_m$ . For example, for the omega-square spectrum ( $n = 2$ ), equation (23) reduces to

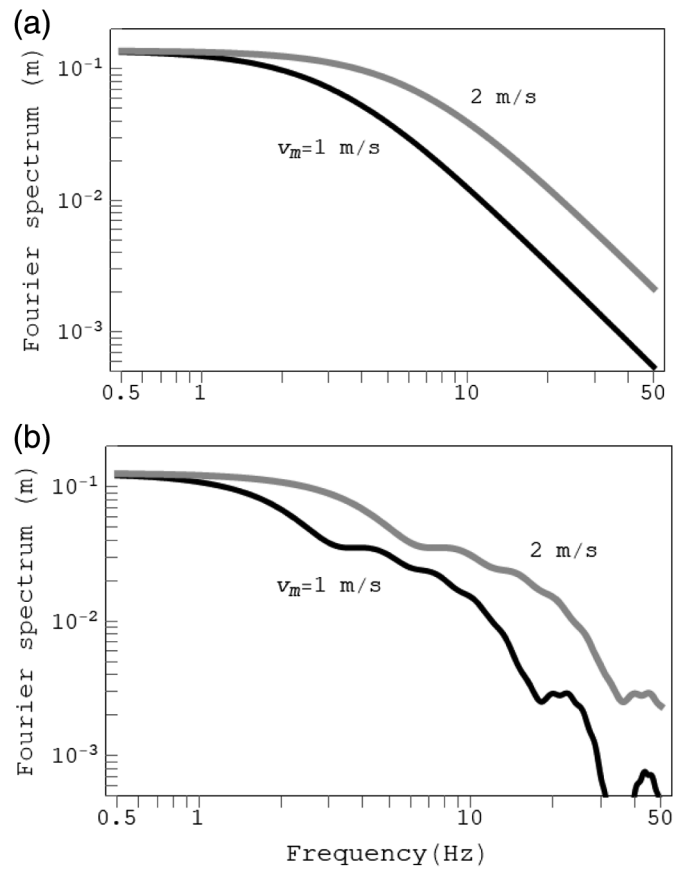


**Figure 7.** Effect of  $v_m$  on the high-frequency levels of the amplitude spectrum of SVF. (a) Spectra of the dimensional  $\omega^2$  SVF for  $v_m = 1$  and 2 m/s. (b) Spectra of the “standard” dimensional pseudodynamic ( $\beta_1 = 0.84$  and  $c = \frac{1}{2}$ ) SVF for  $v_m = 1$  and 2 m/s.

$$|\Delta \dot{u}(\omega)| = e^2 \frac{v_m^2}{U} \omega^{-2}, \quad (24)$$

that is, the spectrum scales as  $v_m^2$ . For the respective Guatteri *et al.* spectrum in equation (16), such a relationship with  $v_m$  is not as obvious but can be checked numerically.

To compare the effect of slip velocities, the dimensional forms of the equations should be used. As an example, Figure 7 compares the effect of doubling the value of  $v_m$  from 1 to 2 m/s on the resulting full amplitude spectra of the dimensional  $\omega^2$  ( $n = 2$ ) SVF (equation 19) and the “standard” dimensional pseudodynamic ( $\beta_1 = 0.84$  and  $c = \frac{1}{2}$ ) SVF (equation 16). The value of  $U = 0.14$  m was again used in the computation. As expected for the  $\omega^2$  spectrum, doubling  $v_m$  leads to the multiplication of the high-frequency spectral values by a factor of four according to equation (24) (Fig. 7a). The same multiplication also occurs for the pseudodynamic spectrum (Fig. 7b), showing complete quantitative equivalence of the dominating role of the maximum slip rate in controlling the strength of high-frequency levels in both models.

## CONCLUSIONS

There is a far-reaching equivalence between the generalized fault SVF, inferred from dynamic rupture simulations by Guatteri *et al.* and the  $\omega^n$  SVF commonly used in kinematic simulations of fault radiation.

Both SVFs are controlled by the same two physical parameters of faulting: the static offset  $U$  and the maximum slip rate  $v_m$ . Two parameters are fundamentally needed, because they exert their primary effect on the low- and high-frequency parts of the spectra, respectively (Beresnev, 2009).

The fault rise times in both models are conveniently expressed through the same two physical parameters and are close numerically. The mutually equivalent additional parameters that affect the rise times are  $\beta_1$  and  $c$  in the dynamic case, on one hand, and  $n$  in the omega- $n$  model, on the other.

The full range of change in the temporal shape of the pseudodynamic source time function, spanning the entire space of parameters, roughly corresponds to the full range of change in the omega- $n$  functions with  $n$  ranging from approximately 1.5 to 3.5. In the Fourier domain, the omega- $n$  model, in which  $n$  changes in a narrower range from approximately 2 to 2.5, covers nearly the entire variety of the possible pseudodynamic spectra.

The value of the peak slip velocity exerts dominant control on the strength of high-frequency radiation in both models. For example, for both the pseudodynamic SVF with Guatteri *et al.*'s preferred shape, on one hand, and the omega-square SVF, on the other, the high-frequency levels scale exactly as  $v_m^2$ .

The inability of the Guatteri *et al.* pseudodynamic SVF to preserve the prescribed static displacement  $U$  on the fault, the amount of error being controlled by the parameter  $\beta_1$ , is its significant disadvantage as compared to the  $\omega^n$  functions.

## DATA AND RESOURCES

No data were used in the article. All inferences were made through the analyses of the respective equations and literature sources as indicated. The reference to Southern California Earthquake Center (SCEC) Broadband Platform (BBP) for Ground-Motion Simulation and Validation is available at [www.scec.org/article/697](http://www.scec.org/article/697) (last accessed March 2022).

## DECLARATION OF COMPETING INTERESTS

The author acknowledges that there are no conflicts of interest recorded.

## ACKNOWLEDGMENTS

The author is indebted to M. Mai and two anonymous referees for the constructive comments.

## REFERENCES

Aagaard, B. T., R. W. Graves, D. P. Schwartz, D. A. Ponce, and R. W. Graymer (2010). Ground-motion modeling of Hayward fault scenario earthquakes, Part I: Construction of the suite of scenarios, *Bull. Seismol. Soc. Am.* **100**, 2927–2944.

Aki, K., and P. G. Richards (1980). *Quantitative Seismology*, W. H. Freeman and Company, San Francisco, California.

Báth, M. (1974). *Spectral Analysis in Geophysics*, Elsevier, Amsterdam, The Netherlands.

Beresnev, I. A. (2001). What we can and cannot learn about earthquake sources from the spectra of seismic waves, *Bull. Seismol. Soc. Am.* **91**, 397–400.

Beresnev, I. A. (2009). The reality of the scaling law of earthquake-source spectra? *J. Seismol.* **13**, 433–436.

Beresnev, I. A. (2019). Interpretation of kappa and fmax filters as source effect, *Bull. Seismol. Soc. Am.* **109**, 822–826.

Beresnev, I. A. (2022). The strongest possible earthquake ground motion, *J. Earthq. Eng.* **26**, 563–572.

Beresnev, I. A., and G. M. Atkinson (1997). Modeling finite-fault radiation from the  $\omega^n$  spectrum, *Bull. Seismol. Soc. Am.* **93**, 67–84.

Boore, D. M. (2003). Simulation of ground motion using the stochastic method, *Pure Appl. Geophys.* **160**, 635–676.

Bronshtein, I. N., K. A. Semendiyayev, G. Musiol, and H. Muehlig (2004). *Handbook of Mathematics*, Fourth Ed., Springer, Berlin, Germany.

Brune, J. N. (1970). Tectonic stress and the spectra of seismic shear waves from earthquakes, *J. Geophys. Res.* **75**, 4997–5009.

Dreger, D. S., and T. H. Jordan (2015). Introduction to the Focus Section on validation of the SCEC Broadband Platform v14.3 simulation methods, *Seismol. Res. Lett.* **86**, 15–16.

Graves, R. W., and A. Pitarka (2010). Broadband ground-motion simulation using a hybrid approach, *Bull. Seismol. Soc. Am.* **100**, 2095–2123.

Guatteri, M., P. M. Mai, and G. C. Beroza (2004). A pseudo-dynamic approximation to dynamic rupture models for strong ground motion prediction, *Bull. Seismol. Soc. Am.* **94**, 2051–2063.

Kanamori, H., and D. L. Anderson (1975). Theoretical basis of some empirical relations in seismology, *Bull. Seismol. Soc. Am.* **65**, 1073–1095.

Liu, P., R. J. Archuleta, and S. H. Hartzell (2006). Prediction of broadband ground-motion time histories: Hybrid Low/High-frequency method with correlated random source parameters, *Bull. Seismol. Soc. Am.* **96**, 2118–2130.

Mena, B., P. M. Mai, K. B. Olsen, M. D. Purvance, and J. M. Brune (2010). Hybrid broadband ground-motion simulation using scattering Green's functions: Application to large-magnitude events, *Bull. Seismol. Soc. Am.* **100**, 2143–2162.

Motazedian, D., and G. Atkinson (2005). Stochastic finite-fault modeling based on a dynamic corner frequency, *Bull. Seismol. Soc. Am.* **95**, 995–1010.

Pitarka, A., R. Graves, K. Irikura, K. Miyakoshi, C. Wu, H. Kawase, A. Rodgers, and D. McCallen (2022). Refinements to the Graves-Pitarka kinematic rupture generator, including a dynamically consistent slip-rate function, applied to the 2019 Mw 7.1 Ridgecrest earthquake, *Bull. Seismol. Soc. Am.* **112**, 287–306.

Skarlatoudis, A. A., P. G. Somerville, H. K. Thio, and J. R. Bayless (2015). Broadband strong ground motion simulations of large subduction earthquakes, *Bull. Seismol. Soc. Am.* **105**, 3050–3067.

Tinti, E., E. Fukuyama, A. Piatanesi, and M. Cocco (2005). A kinematic source-time function compatible with earthquake dynamics, *Bull. Seismol. Soc. Am.* **95**, 1211–1223.

Wells, D. L., and K. J. Coppersmith (1994). New empirical relationships among magnitude, rupture length, rupture width, rupture area, and surface displacement, *Bull. Seismol. Soc. Am.* **84**, 974–1002.